Three-dimensional micro structured nanocomposite beams by microfluidic infiltration

L L Lebel [1], B Aissa [2], O A P Monroy [1], M A El Khakani [2] and D Therriault[1]

[1] Center for Applied Research on Polymers (CREPEC) Mechanical Engineering Department, École Polytechnique de Montréal, P.O. Box 6079, Station "Centre-Ville", Montreal, Canada, H3C 3A7, phone: 514-340-4711 x4419, fax: 514-340-4176
[2] National Institute of Scientific Research - Energy, Materials, and Telecommunications, 1650 Blvd. Lionel-Boulet, Varennes, QC, J3X 1S2 Canada, phone: 450-929-8122, fax: 450-929-8120

E-mail: daniel.therriault@polymtl.ca

Abstract. *Three-dimensional (3D) micro structured beams reinforced with single walled carbon nanotube (C-SWNT)/polymer nanocomposite were fabricated by using an approach based on the infiltration of 3D microfluidic networks. The 3D microfluidic network was first fabricated by the direct-write assembly method, which consists of robotized deposition of fugitive ink filaments on an epoxy substrate, forming thereby a 3D micro structured scaffold. After encapsulating the 3D micro-scaffold structure with an epoxy resin, the fugitive ink was liquefied and removed, resulting in a 3D network of interconnected microchannels. This microfluidic network was then infiltrated by polymer loaded with C-SWNTs and subsequently cured. Prior to their incorporation in the polymer matrix, the UV-laser synthesized C-SWNTs were purified, functionalized and dispersed into the matrix by using a three-roll mixing mill. The final samples consist of rectangular beams having a complex 3D-skeleton structure of C-SWNT/polymer nanocomposite fibers, adapted to offer better performance under flexural solicitation. Dynamic mechanical analysis in flexion showed an increase of 12.5% in the storage modulus under 35°C compared to the resin infiltrated beams. The nanocomposite infiltration of microfluidic networks demonstrated here opens new prospects for the achievement of 3D reinforced micro structures.*

Submitted to: Journal of Micromechanics and Microengineering

1. Introduction

Single-walled carbon nanotubes [1,2] (C-SWNT) nanocomposites with polymer matrices receive much attention due to their high potential for application as actuators in microelectromechanical systems [3,4], strain and damage sensing [7], electroactive shape-memory polymers [8], or electrostatic discharge and electro-magnetic radio interference protection [9]. Nevertheless, several challenges have still to be addressed in order to obtain a functional product using C-SWNTs reinforced polymer nanocomposites. First, a controlled synthesis of high-quality C-

SWNTs, with the highest aspect ratio possible and preferably the less-entangled possible has to be developed. Second, the nanotubes have to be appropriately dispersed in the polymer matrix. Third, a chemical interaction between the host polymer and the C-SWNTs is a prerequisite to ensure their appropriate anchoring with the polymer. Finally, the spatial orientation and layout of the axisymmetric reinforcement in a final product should be controlled for optimal mechanical reinforcement. To improve the dispersion of C-SWNTs, one possible approach is to use a non-covalent attachment of large π-system molecules such as zinc protoporphyrin IX [10] to C-SWNT wall. It has also been reported that acid treatments could introduce carboxyl groups along the tube walls [11]. This covalent modification of the nanotubes can significantly improve the dispersion, chemical, and mechanical interactions with polymers containing polar units in their backbone such as polyurethane [12]. To address the problem of C-SWNTs orientation, shear flow [13] and electromagnetic fields [14,15] along with dimensional constraints have proven their efficiency. To constrain C-SWNT orientation in 2D, compression molding of films or solvent casting of films techniques have been employed. To constrain the nanotube orientation in 1D, film extrusion, fiber spinning [16] and stretching, and fiber electrospinning [17] are among the approaches used so far. A passive approach was proposed where the nanocomposite was infiltrated in a 2D microfluidic system [18], that was created with the direct-write assembly of fugitive ink [19]. The resulting nanocomposite product had an internal micro-structure composed of 2 sets of parallel axial fibers separated by a substrate. Nevertheless, none of these techniques have successfully generated a final product with sufficient control on the three dimensional (3D) orientation and/or positioning of the nanotube reinforcement. In general, additional subsequent manufacturing steps are necessary to tailor the 3D layout of the nanocomposite fibers in the final product.

In this article, we propose an original approach which permits the fabrication of a 3D-reinforced product through the directed and localized infiltration of C-SWNT/polymer nanocomposites into a 3D microfluidic network. The reinforcing skeleton can be tailored at will by using the highly-flexible direct-write assembly method [19]. Figure 1 illustrates how the fugitive ink can be used to manufacture a 3D microfluidic scaffold network (Figure 1a-d). Infiltration of the scaffold network with a C-SWNT/polymer nanocomposite fluid (Figure 1e) and its subsequent curing allows the fabrication of 3D-reinforced nanocomposite structures (Figure 1f). On the other hand, at the structural level, stress concentration will not occur due to the circular cross-section of the produced microfluidic channels. Flexural mechanical solicitation generates an axial stress distribution that linearly increases from the neutral mid-plane until reaching a maximum value at the outer surfaces. Thus, by using the technique depicted in Figure 1, nanocomposite reinforced rectangular beams were manufactured where the number of the axial reinforcing infiltrated microfibers was increased in higher stress regions of the cross-section. The infiltrated nanocomposite was a blend of laser ablated C-SWNTs incorporated in a polyurethane matrix. The morphology of the beams was

characterized using optical microscopy. The mechanical properties of the fabricated 3D-reinforced nanocomposite beams were characterized by means of a dynamic mechanical analyzer (DMA).

2. Experimental

The C-SWNT material was produced by using the UV-laser ablation of a graphite target appropriately doped with Co/Ni metal catalyst, under a controlled Argon atmosphere at a furnace temperature of 1100°C (more details on the C-SWCNTs were reported elsewhere [20]). The as-grown C-SWNTs were purified by subjecting them to an acidic treatment where they were oxidized through refluxing in a 3M-HNO_3 (Sigma Aldrich) solution for 5 hours at 130° C and subsequently filtered (Filter type-GV, Millipore corp.). The nanostructural characteristics of the purified nanotubes were examined by means of bright field transmission electron microscopy (TEM) imaging by using a Jeol JEM-2100F FEG-TEM (200 kV) microscope. The C-SWNTs were also systematically analyzed by means of Raman spectroscopy (microRaman, Renishaw Imaging Microscope Wire), in the backscattering geometry, using the 514.5 nm wavelength of an Ar^+ laser as an excitation line. X-ray photoelectron spectroscopy (XPS, Escalab 220i-XL, VG instruments) was used to characterize the chemical bonding of C-SWNTs samples.

The nanocomposite material was a mixture of C-SWNTs with a commercially available polyurethane matrix (NEA123MB, Norland Products) containing a UV photoinitiator active at 365nm and a heat catalyst active at 60° C. The weighted amount of C-SWNT was first dispersed in a solution of 0.1 mM of zinc protoporphyrin IX (ZnPP, Sigma-Aldrich) in dichloromethane (DCM, Sigma-Aldrich). After ultrasonication (Ultrasonic cleaner 8891, Cole-Parmer) for 30 minutes, polyurethane was slowly added in this solution over a stirring hot plate (Model SP131825, Barnstead international). After solvent evaporation under vacuum, the resulting nanocomposite containing a 0.005 mass fraction (0.5 wt%) of C-SWNT inside polyurethane was passed several times in a three-roll mixing mill (Exakt 80E, Exakt Technologies Inc.) where the gap between the rolls and the speed of the apron roll were adjusted according to the method described by Thostenson and Chou [21]. The total procedure consisted of 5 passes at a gap of 25 μm and with a speed of 200 RPM, 5 passes at a gap of 15 μm with a speed 200 RPM and finally 9 passes at a gap of 5 μm with a speed 250 RPM. The microscopic scale dispersion was characterized by observing a ~100 μm thick film under transmission light optical microscope using the 40X objective (BX-61, Olympus) and image analysis software (Image-Pro Plus, Media Cybernetics Inc). The nanoscopic scale dispersion was assessed using TEM observations on cryogenically microtomed slices of cured nanocomposites.

The microfluidic networks were fabricated by depositing a fugitive ink filament scaffold structure in a layer by layer fashion (as illustrated in Figure 1a-d) on a 1 mm thick epoxy substrate (Epon 828 / Epikure 3274, Miller-Stephenson Chemical Co.). The fugitive ink was a 30 wt% binary

mixture of microcrystalline wax (SP 18, Strahl & Pitstch) in a lower M_w organic phase (Vaseline petroleum jelly, Lever Pond's) [22]. The deposition system consists of a computer controlled robot (I & J2200-4, I & J Fisnar) that moved a dispensing apparatus (HP-7X, EFD) along the *x*, *y* and *z* directions. The filament diameter was of ~180 μm. The overall dimensions of the deposited scaffold were 55 mm in length, 4.7 mm in width and 1.32 mm in thickness. The scaffold consisted of 9 layers of fugitive ink filaments, deposited alternatively along and perpendicular to the beam longitudinal axis. The incremental vertical distance between the layers was 80% of the filament diameter to insure a good connection between the layers. In addition, the number of longitudinal filaments in their respective layers changed depending on the layer position in the stack. The first and ninth layers comprised 16 filaments, the third and seventh layers had 12 filaments, and the central layer (fifth) had 8 filaments. The velocity of the dispensing apparatus was 5.8 mm/s, and the pressure for extruding the fugitive ink was set at 1.4 MPa for a total deposition time of a few minutes. After deposition, the scaffold was encapsulated into epoxy resin that was cured at room temperature. The microfluidic network was finally obtained after heating the whole construction at 80°C and applying vacuum to remove the liquefied fugitive ink.

Using the drained microfluidic networks as a support, reinforced beams were produced by infiltrating C-SWNT/polyurethane nanocomposite (0.5 wt%) or pure polyurethane (0 wt%) inside the microchannel networks. Shortly after filling of the channels, the beam was exposed to 365 nm ultraviolet light provided by a UV lamp (High intensity UV lamp, Cole-Parmer Canada Inc.) for 5 minutes. Empty, resin- and nanocomposite-reinforced beams were then post-cured at 90° C for three hours. Finally, four beams of each kind were cut and polished to test dimensions (i.e. ~55 mm-long, ~5.5 mm-wide and ~1.8 mm-thick). The morphology of the beams was observed under optical microscopy.

The beam effective complex modulus ($E^* = E' + iE''$ where E' is the storage modulus and E'' is the loss modulus) was measured under a dynamic mechanical analyzer (DMA 2980, TA instruments) over the 0-100 °C temperature range. A temperature ramp of 4° C/min was applied at a frequency of 10 Hz with an amplitude of 25 μm. Pure epoxy and polyurethane coupons were also tested under the same conditions in order to identify their glass transition temperature (T_g), taken as the peak of the E'' curve.

3. Results and discussion

Prior their incorporation inside the polyurethane matrix, the laser-ablated material was characterized using various techniques. Figure 2 shows a TEM micrograph of the purified laser-synthesized deposits, where bundles of C-SWNTs are clearly seen to consist of few single-walled nanotubes. In conjunction with the C-SWNTs, other carbon nanostructures (nanocages, nanonions,

nanohorns, etc…) can be also produced by the laser process, as previously reported [20]. Some of these C nanostructures can also visible in Figure 2. These C-SWNTs feature a very high aspect ratio (up to 10^3) as their length can easily reach up to several micrometers and their diameter is in the nanometer range (bundles of ~ 2 to 10 nm-diameter and a C-SWNTs-diameter of ~1.2 nm were observed in the present case. A typical Raman spectrum (Figure 3a) of the purified C-SWNTs shows clear scattering peaks appearing in the low (100-300 cm^{-1}) and high (~1600 cm^{-1}) frequency regions, corresponding to the radial breathing mode (RBM) and the tangential vibrating mode (G), respectively, which are the fingerprint of the presence of C-SWNTs. The RBM peak centered at 182 cm^{-1} is attributed to the strong presence of C-SWNTs having a mean diameter of 1.2 nm according to the formula of Bandow et al. [23]. The D peak centered around 1350 cm^{-1} is due to the presence of amorphous and/or disordered carbon structures (part of which might be produced during the acidic oxidization treatment). Nevertheless, it is worth noting the rather high G-to-D peak intensity ratios, which indicates the overall good-quality of the C-SWCNTs. The bonding state of the purified C-SWNTs deposits were also characterized by high-resolution XPS, as shown in Figure 3b which shows the C1s core level spectrum of the purified C-SWNTs. The C1s peak was found to consist of three clear components. Indeed, in addition to the main component centered around 284.5 eV (which is due to the sp^2 C=C bonding forming the bulk structure of C-SWNTs), the two shoulders appearing at 286 eV and 288 eV can be attributed to C-O bonds and to COO group of carboxylic acid groups, respectively [24,25]. These bonds are thought to be formed during the nitric acid based purification process. The covalent functionalization, revealed here by the XPS measurements, is expected to improve the dispersion and enhance the chemical (and hence mechanical) interaction of the C-SWNTs with the polyurethane host matrix.

To assess the quality of the blending process used, a 10 μm film of the C-SWNTs/polyurethane blend was deposited, cured and observed under transmission optical microscopy. Figure 4a shows the optically transparent polyurethane film where dark spots are observed. These spots (of which average size was estimated to ~1.4 μm) are believed to be aggregates of carbonaceous materials. Based on these observations, which does not pretend to be exhaustive, the whole incorporation process involving carboxylic groups graphing on C-SWNT during purification, a solubilization using the ZnPP non-covalent functionalization, and the high shear mixing using the three-roll mixer was efficient to obtain a fairly uniform dispersion at the microscopic scale. In attempt to gain more insight on the dispersion of C-SWNTs into the polyurethane matrix at the nanoscale, we have performed TEM observations on ultrathin slices of the nanocomposite. Some nanoaggregates (as illustrated in Figure 4b), probably consisting of few entangled C-SWNTs, were found in the polymer matrix. This observation indicates a certain degree of successful integration of the C-SWNTs inside the polyurethane matrix.

The nanocomposite was subsequently infiltrated in the microfluidic networks obtained after cleaning the fugitive ink inside the cured epoxy beams. Figure 5a shows an isometric view of the nanocomposite reinforced beam and Figure 5b its cross-section where the five layers of longitudinal reinforcing fibers are seen as dark circles of 180µm in diameter separated by four intermediate layers of perpendicular fibers. The repartition of the longitudinal fibers varies along the sample thickness and faithfully reproduces the original microfluidic network design. The quantity of fibers is higher near the top and bottom surfaces where axial stress resulting from flexural solicitation is greater. Figure 5c shows top views of the beams at different infiltration conditions, namely the non-infiltrated beam (Empty), the beam solely infiltrated by pure polyurethane (0 wt%), and the C-SWNT/polyurethane nanocomposite infiltrated beam (0.5 wt% of C-SWNTs in the polyurethane matrix) The microfluidic channels can be observed through the surface of the empty beam. As the refractive index of the polyurethane reinforcement is similar to that of the epoxy envelope composing the beam, the internal microstructure of the polyurethane (0 wt%) infiltrated beam is barely visible. On the contrary, black orthogonal lines are observed through the surface of the nanocomposite infiltrated beam representing the longitudinal and perpendicular reinforcing nanocomposite fibers. The observation of the reinforced beam can also lead to the conclusion that the infiltration and curing conditions yield to a complete filling of the microfluidic network because no voids (or empty portions of channels) are seen.

The effective complex flexural modulus E^* measured under DMA was separated in its real part (E'), indicating the capacity of the beam to store and return energy, and its imaginary part (E''), which quantify the aptitude of the beams to lose and dissipate energy in friction and internal motion. Figure 6 shows the temperature dependence of the effective E' and E'' of the empty, polyurethane (0 wt%) and nanocomposite reinforced (0.5 wt%) beams, as obtained from the dynamic mechanical analysis. The empty beam E' undergoes a constant rate decrease until 60° C near the epoxy T_g, indicated by a single peak in E'' curve. For the reinforced beams, E' also decreases with the temperature until a major drop is observed at ~ 60° C. However, the decreasing rates of the E' curves change because of the polyurethane transition to a rubbery behavior, being a constituent of the infiltrated fibers in both the 0 wt% and 0.5 wt% reinforced beams. These different slopes in the E' curves are related to peaks in the corresponding E'' curves, shown at Figure 6b. A T_g of 60° C was measured for the pure epoxy and a T_g of 35° C was measured for the pure polyurethane using DMA with similar conditions. Below the glass transition temperature of the polyurethane, an increase in E' of 12.5% is observed for the nanocomposite (0.5 wt%) reinforced beams compared to the unloaded-polyurethane reinforced beams (0 wt%). Such an increase in E' is attributed here to the reinforcing effect of the C-SWNTs in accordance with the beneficial effect on the elastic modulus observed when loading polymers with C-SWNTs [26]. Another important observation is made concerning the higher

E'' of the nanocomposite and polyurethane reinforced beams in comparison with the empty beams. Energy dissipation in friction might be occurring at the interface between the rigid infiltrated fibers and their epoxy sheath during mechanical solicitation. A poor mechanical shear stress transfer would be caused by both residual traces of fugitive ink (that acts as a lubricant) and the probable shrinkage-induced detachment of the fiber surface from the microfluidic channel walls.

4. Conclusion

Three dimensional microstructured reinforced beams have been manufactured using an original approach based on the nanocomposite infiltration of a microfluidic network. The resulting product is a nanocomposite beam of which the structure of its reinforcing fiber network can be tailored at will in the three-dimensions. The preliminary mechanical characterization performed here showed that the nanocomposite infiltrated beams have higher storage modulus due to the C-SWNTs reinforcement. However, a more systematic study comparing various C-SWNT concentrations is to be undertaken to establish the optimal reinforcement conditions. For the C-SWNTs, a more sophisticated purification methods permitting the exfoliation and separation of the nanotubes (ideally isolated tubes) has to be investigated. Finally, it is worth noting that the higher damping properties of these reinforced structures, as reflected by a higher loss modulus, may be useful in products where vibration absorption and management are important. Because of the wide range of viscosities and types of nanoreinforcements that could be used, the infiltration of complex microfluidic scaffolds represents a highly flexible technique for the achievement of a variety of functional 3D reinforced nanocomposite macroscopic products.

5. ACKNOWLEGEMENTS

The authors acknowledge the financial support from FQRNT (Le Fonds Québécois de la Recherche sur la Nature et les Technologies) and NSERC (the Natural Sciences and Engineering Research Council of Canada). The authors thank Prof. Charles Dubois for his help and thoughtful discussions on the C-SWNTs/polymer nanocomposite processing. They also acknowledge the support of Profs. Nakai and Hamada (Kyoto Institute of Technology) for permitting some of the mechanical tests in their laboratory. Finally, we thank Ms. Leelapornpisit and M. Masse for their collaboration in performing the TEM observations.

6. Figures

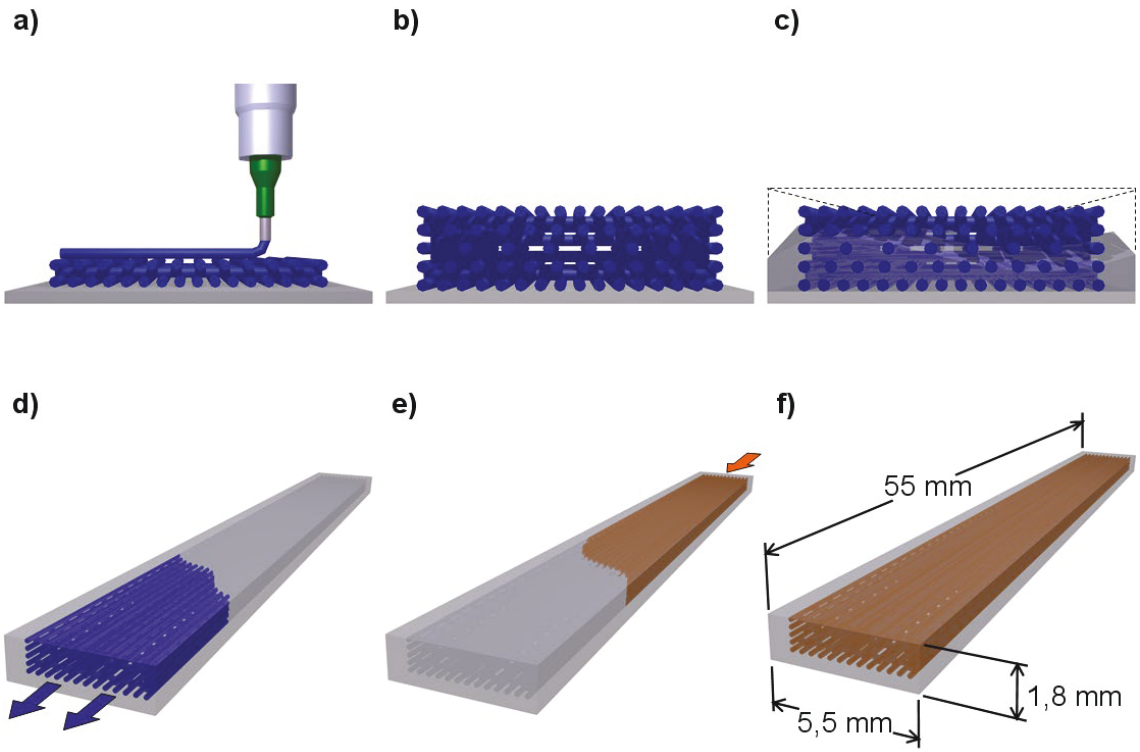

Figure 1. Schematic illustration of the manufacturing process of a microfluidic infiltrated beam. (a) Direct-write of fugitive ink scaffold on a epoxy slide. (b) The fugitive ink scaffold has different numbers of longitudinal fibers depending of the layer. (c) Encapsulation of the 3D network using epoxy resin. (d) Removal of the liquefied fugitive ink at moderate temperature (T = 80°C). (e) Infiltration of the network by the nanocomposite reinforcement followed by curing. (f) Cut beam to final dimensions.

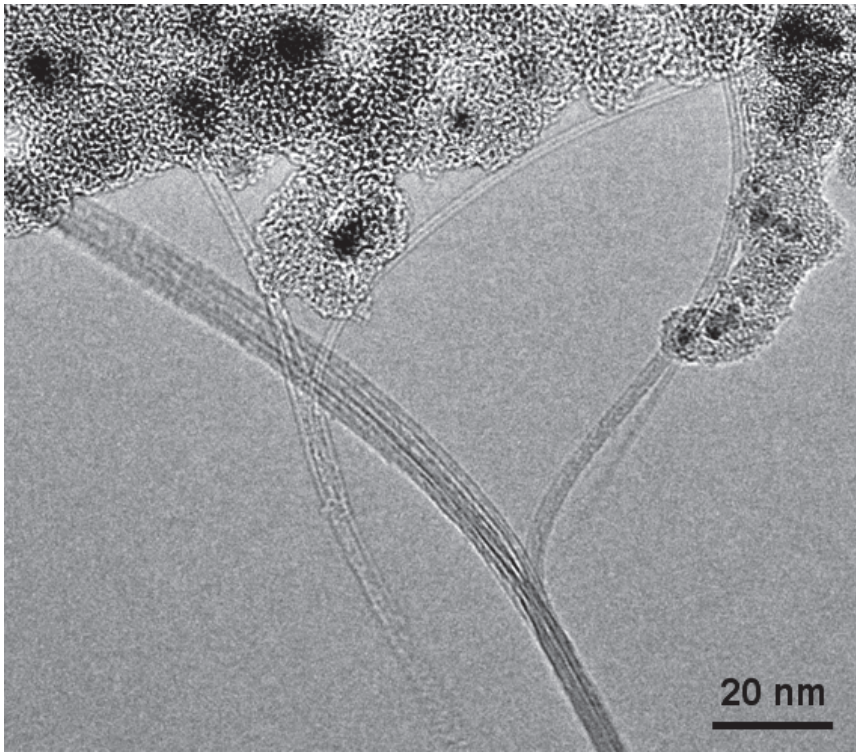

Figure 2. TEM image of the purified C-SWNT deposit.

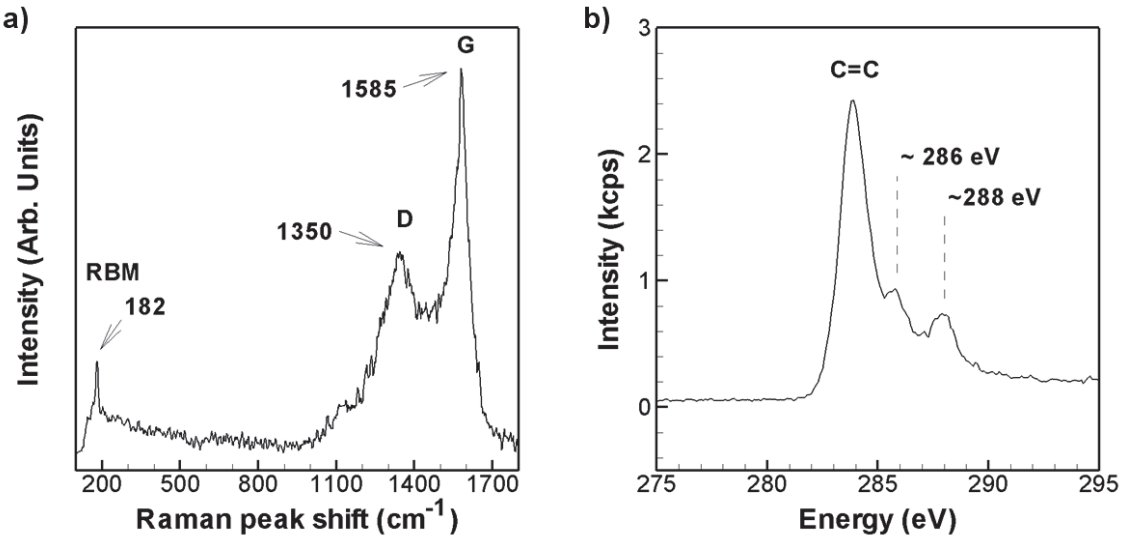

Figure 3. Spectroscopic characterizations of the C-SWNTs. (a) typical Raman spectrum of purified C-SWNTs. (b) X-ray Photoelectron spectrum of C1s core level of purified C-SWNTs.

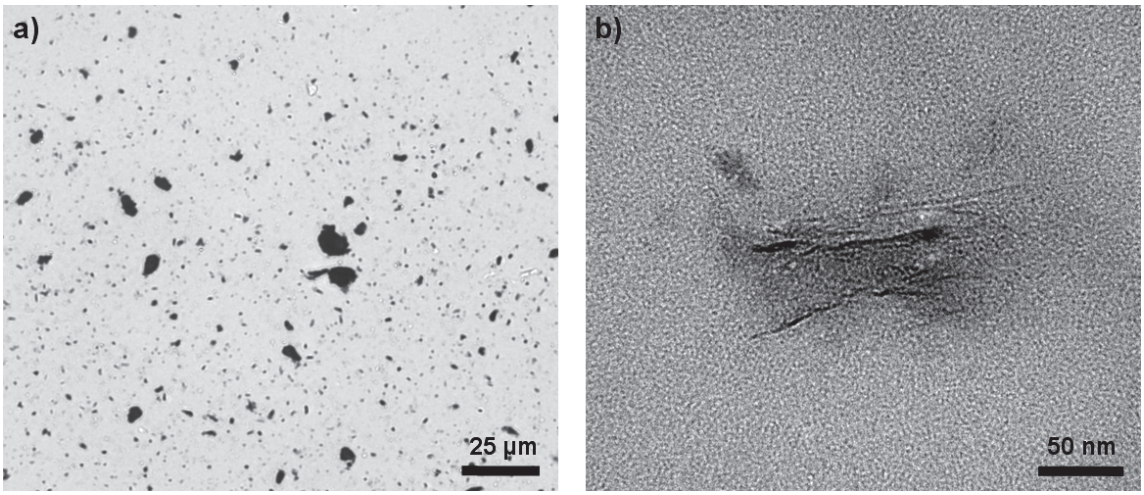

Figure 4. (a) Optical microscope image of a 10 µm thick film of C-SWNTs/polyurethane nanocomposite blend. (b) TEM micrograph taken on a microtomed slice of C-SWNTs/polyurethane nanocomposite.

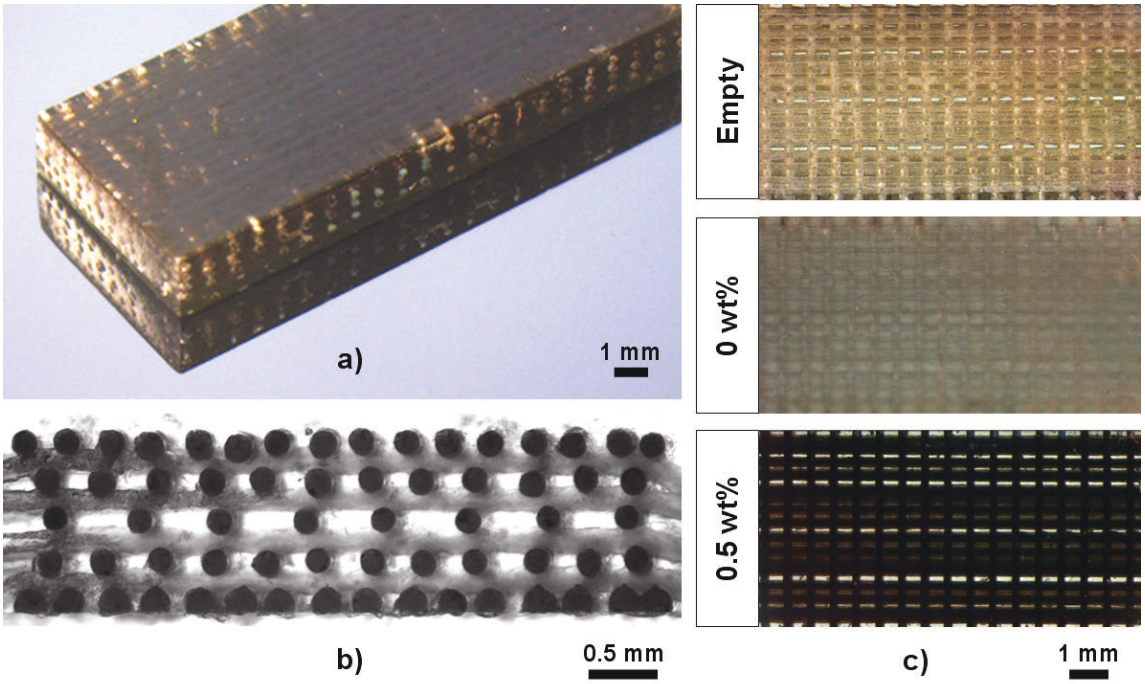

Figure 5. Morphology of the microfluidic infiltrated beams. (a) Partial Isometric view of a 0.5wt% C-SWNT/polyurethane nanocomposite infiltrated beam. (b) Typical cross-section of a microfluidic infiltrated beam. (c) Top view of microfludic beams showing the different infiltration conditions: no infiltration (empty), pure polyurethane infiltration (0 wt%), and C-SWNT/polyurethane nanocomposite infiltration (0.5 wt%).

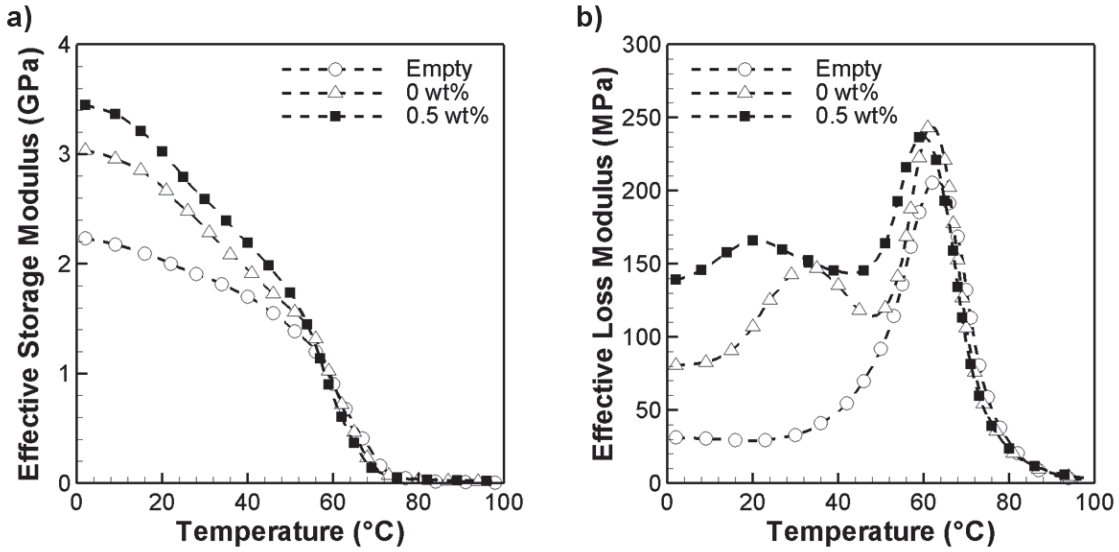

Figure 6. Microfluidic infiltrated beams storage (a) and loss (b) modulus for different conditions: empty, infiltrated with pure polyurethane resin (0 wt%) and infiltrated with C-SWNT/polyurethane nanocomposite (0.5 wt%).

7. REFERENCES

[1] Bethune D S, Kiang C H, de Vries M S, Gorman G, Savoy R, Vazquez J and Beyers R 1993 Cobalt-catalysed growth of carbon nanotubes with single-atomic-layer walls *Nature* **363** 605

[2] Iijima S and Ichihashi T 1993 Single-shell carbon nanotubes of 1-nm diameter *Nature* **364** 737

[3] Lu S and Panchapakesan B 2007 Photomechanical responses of carbon nanotube/polymer actuators *Nanotechnology* **18**

[4] Ashrafi B, Hubert P and Vengallatore S 2006 Carbon nanotube-reinforced composites as structural materials for microactuators in microelectromechanical systems *Nanotechnology* **17** 4895-903

[5] Qian D, Wagner G J, Liu W K, Yu M-F and Ruoff R S 2002 Mechanics of carbon nanotubes *Appl. Mech. Rev.* **55** 495-532

[6] Tans S J, Devoret M H, Dai H, Thess A, Smalley R E, Georliga L J and Dekker C 1997 Individual single-wall carbon nanotubes as quantum wires *Nature* **386** 474-7

[7] Thostenson E T and Chou T-W 2006 Carbon nanotube networks: Sensing of distributed strain and damage for life prediction and self healing *Adv. Mater.* **18** 2837-41

[8] Sahoo N G, Jung Y C, Yoo H J and Cho J W 2007 Influence of carbon nanotubes and polypyrrole on the thermal, mechanical and electroactive shape-memory properties of polyurethane nanocomposites *Compos. Sci. Technol.* **67** 1920-9

[9] Sandler J K W, Kirk J E, Kinloch I A, Shaffer M S P and Windle A H 2003 Ultra-low electrical percolation threshold in carbon-nanotube-epoxy composites *Polymer* **44** 5893-9

[10] Murakami H and Nakashima N 2006 Soluble carbon nanotubes and their applications *J. Nanosci. Nanotechno.* **6** 16-27

[11] Salernitano E, Giorgi L, Dikonimos Makris T, Giorgi R, Lisi N, Contini V and Falconieri M 2007 Purification of mwcnts grown on a nanosized unsupported fe-based powder catalyst *Diam. Relat. Mater.* **16** 1565-70

[12] Sahoo N G, Jung Y C, Yoo H J and Cho J W 2006 Effect of functionalized carbon nanotubes on molecular interaction and properties of polyurethane composites *Macromol. Chem. Physic.* **207** 1773-80

[13] Thostenson E T and Chou T-W 2002 Aligned multi-walled carbon nanotube-reinforced composites: Processing and mechanical characterization *J. Phys. D Appl Phys.* **35** 77-80

[14] Kimura T, Ago H, Tobita M, Ohshima S, Kyotani M and Yumura M 2002 Polymer composites of carbon nanotubes aligned by a magnetic field *Adv. Mater.* **14** 1380-3

[15] Park C, Wilkinson J, Banda S, Ounaies Z, Wise K E, Sauti G, Lillehei P T and Harrison J S 2006 Aligned single-wall carbon nanotube polymer composites using an electric field *J. Polym. Sci. Pol. Phys.* **44** 1751-62

[16] Sandler J K W, et al. 2004 A comparative study of melt spun polyamide-12 fibres reinforced with carbon nanotubes and nanofibres *Polymer* **45** 2001-15

[17] Ko F, Gogotsi Y, Ali A, Naguib N, Ye H, Yang G, Li C and Willis P 2003 Electrospinning of continuous carbon nanotube-filled nanofiber yarns *Adv. Mater.* **15** 1161-5

[18] Lebel L L, Aissa B, Khakani M A E and Therriault D, *Tridimensional microstructures of swcnt reinforced polymer nanocomposite by means of a microfluidic infiltration approach*, in *2007 MRS Fall Meeting*. 2007: Boston, MA.

[19] Therriault D, White S R and Lewis J A 2003 Chaotic mixing in three-dimensional microvascular networks fabricated by direct-write assembly *Nat. Mater.* **2** 265-71

[20] Braidy N, El Khakani M A and Botton G A 2002 Carbon nanotubular structures synthesis by means of ultraviolet laser ablation *J. Mater. Res.* **17** 2189-92

[21] Thostenson E T and Chou T-W 2006 Processing-structure-multi-functional property relationship in carbon nanotube/epoxy composites *Carbon* **44** 3022-9

[22] Therriault D, Shepherd R F, White S R and Lewis J A 2005 Fugitive inks for direct-write assembly of three-dimensional microvascular networks *Adv. Mater.* **17** 395-9

[23] Bandow S, Asaka S, Saito Y, Rao A M, Grigorian L, Richter E and Eklund P C 1998 Effect of the growth temperature on the diameter distribution and chirality of single-wall carbon nanotubes *Phys. Rev. Lett.* **80** 3779-82

[24] Baker S E, Cai W, Lasseter T L, Weidkamp K P and Hamers R J 2002 Covalently bonded adducts of deoxyribonucleic acid (DNA) oligonucleotides with single-wall carbon nanotubes: Synthesis and hybridization *Nano Lett.* **2** 1413-7

[25] Okpalugo T I T, Papakonstantinou P, Murphy H, McLaughlin J and Brown N M D 2005 High resolution xps characterization of chemical functionalised mwcnts and swcnts *Carbon* **43** 153-61

[26] Coleman J N, Khan U, Blau W J and Gun'ko Y K 2006 Small but strong: A review of the mechanical properties of carbon nanotube-polymer composites *Carbon* **44** 1624-52